HydroResearch 5 (2022) 1–12

Contents lists available at ScienceDirect

HydroResearch

journal homepage: http://www.keaipublishing.com/en/journals/hydroresearch/

Spatial variation of sub-surface heterogenieties within the dyke swarm of Nandurbar region, Maharashtra, India, for groundwater exploration using Inverse Distance Weighted technique

Khan Tahama [a], Arti Baride [b], Gautam Gupta [a,*], Vinit C. Erram [c], Mukund V. Baride [b]

[a] Indian Institute of Geomagnetism, New Panvel (W), Navi Mumbai 410218, India
[b] Dept. of Geology, Z.B. Patil College of Arts, Science and Commerce, Dhule 424002, India
[c] MF Radar Facility Centre, IIG, Shivaji University Campus, Kolhapur 416004, India

ARTICLE INFO

Article history:
Received 15 December 2020
Received in revised form 1 July 2021
Accepted 17 December 2021
Available online 22 December 2021

Keywords:
ArcGIS
Inverse Distance Weighted
Dar-Zarrouk parameters
Dyke swarm
Nandurbar
India

ABSTRACT

To understand the protective capacity of aquifers, anisotropic nature and fracture geometry of dyke infested terrain in parts of Nandurbar region, Maharashtra, data from 39 vertical electrical soundings using Schlumberger configuration were acquired. Analysis suggests 3–5 layered structure in the study area. Further, the Dar-Zarrouk and other geoelectric indices were computed utilizing resistivity and layer thickness at each station. The Inverse Distance Weighted (IDW) algorithm was used to interpolate data spatially. Longitudinal conductance values suggest that the area has poor to moderate aquifer protective capacity, indicating that weaker zones may be prone to infiltrating contaminants. The high electrical anisotropy (λ) signifies EW and NS oriented dykes, suggesting heterogeneous and anisotropic nature of the subsurface. A direct relationship involving λ and fracture porosity indicate porous medium. The IDW algorithm, used for the first time in this region, provided an accurate and reliable estimate of spatial distribution and the underlying heterogeneities.

1. Introduction

Dykes of the Deccan Volcanic Province (DVP) in Maharashtra are important geological features. The significance of dykes with respect to the hydrogeological set up in a hard rock environment like DVP is not properly recognized. Several studies have been carried out over these features pertaining to its mineralogy, geochemistry, their mode of emplacement, phases of intrusion and palaeomagnetism (Sethna et al., 1996; Melluso et al., 1999; Auden, 1949; Patil and Rao, 2002). Nevertheless, the disposition of dykes in the incidence and movement of groundwater is a subject of debate amongst hydrogeologists (Singh and Jamal, 2002; Babiker and Gudmundsson, 2004; Duraiswami, 2005). This is more pertinent in the areas with acute water shortage, and Nandurbar district in northern Maharashtra is no exception to water scarcity. Thus the need of the hour is to locate secondary sources of groundwater for exploration within the dyke swarms. Nandurbar district of Maharashtra is situated in the southern part of Narmada-Tapi rift zone. Here numerous doleritic dykes and dyke swarms occur as parallel to sub parallel bodies, forming linear ridges of moderate relief. These are partially exposed and in several places they are partly concealed, thus affecting the topography (Geological Survey of India (GSI), 2001).

A few geophysical studies were carried out over the dyke swarm region of Nashik, Dhule and Nandurbar in northern Maharashtra in order to identify conduit and barrier type stretches of dykes and depths to which dykes clutch potential to store and transmit water (Pawar et al., 2008; Erram et al., 2010; Gupta et al., 2012; Tahama et al., 2019). Electrical resistivity is a non-intrusive technique and is commonly used for various purposes: groundwater contamination studies (Mondal et al., 2013), saline water incursion studies (Maiti et al., 2013; Rai et al., 2013; Suneetha et al., 2020), geothermal explorations (Kumar et al., 2011), to delineate the subsurface strata and bedrock zone for construction of suitable groundwater structures and environmental studies (Loke, 2000). Aquifers in vesicular and fractured zones within the trap sequence and sedimentary formations below the traps are thought to be potential groundwater zones (Rai et al., 2013; Shailaja et al., 2019).

Several researchers were of the view that dykes can act as carrier or barrier to the groundwater flow depending upon intensity of fracturing in the dyke rock, their structure, location and direction with regard to the groundwater flow (Singh and Jamal, 2002; Nilsen et al., 2003; Babiker and Gudmundsson, 2004). Pawar et al. (2008) and subsequently Gupta et al. (2012) advocated for the first time that a single dyke can act as haulier or hurdle along its length, an observation that disagrees from earlier studies which report them either completely conduit or barrier type.

* Corresponding author.
E-mail address: gautam.g@iigm.res.in (G. Gupta).

https://doi.org/10.1016/j.hydres.2021.12.001

Notwithstanding the above arguments, the present study portrays the subsurface features over the dyke swarms in parts of Nandurbar district derived from vertical electrical sounding (VES) studies. The objective is also to identify groundwater resource potential in the regional dyke rock aquifer setup in GIS environment. Geophysical parameters like, total longitudinal unit conductance (S), and total transverse unit resistance (T) were computed. Also known as Dar Zarrouk (DZ) parameters, they are related to different combinations of thickness and resistivity for each medium and applied to classify different groundwater characteristics and geological conditions (Batayneh, 2013).

2. Study area: geology and hydrogeology

Nandurbar is an administrative district in the northwest corner of Maharashtra state in India occupying an area of about 6000 km^2. The southern and south-eastern side of this district is encompassed by the Dhule district, the state of Gujarat lies towards west and north while Madhya Pradesh state is located on the north and north-east. The Tapi and Narmada Rivers flows on the northern part of Nandurbar district. The district comprises of six subdivisions, viz. Akkalkuwa, Akrani, Taloda, Shahada, Nandurbar and Navapur. Physiographically, the district is broadly divided into four units i.e., Satpura hills, Tapi River Valley, dykes and residual hills of the Sahyadri, and Nawapur and western Nandurbar region with a westerly feature below the Sahyadri scarps. Coarse shallow soils, medium deep soils and deep black soils characterize the region.

The district has three distinct seasons: summer, monsoon/rainy and the winter season. Summer season is from March to mid of June and are usually sweltering. During the month of May the summer is at its peak with temperatures as high as 45 °C. The monsoon sets in during mid or end of June with marked rainfall in the western part. The average annual rainfall is 767 mm through the district. Winter is from the month of November to February, which is mildly cold but arid.

The Nandurbar region is covered by basaltic lava flows of the Deccan Trap of Upper Cretaceous-Lower Eocene age. An expansive strip of alluvium along the Tapi River is seen in parts of Taloda, Shahada and Nandurbar subdivisions (Fig. 1a). A small patch of Bagh bed sediments of Middle to Upper Cretaceous age is exposed in north-western part of the district. The basaltic lava pile in the north and south of the Tapi River is grouped under Satpura and Sahyadri groups respectively. Bagh beds occur as inliers within the Deccan trap in the NW part (Deshpande, 1998). A stratigraphy map of the study area is shown in Fig. 1b. Broadly, the study area can be stratigraphically grouped as a Lower Ratangarh formation, Upper Ratangarh formation and Quartenary to Recent sediments (Sheth et al., 2018). About 15% of the district are encompassed by Tapi alluvium consisting of clay, silt, sand, gravels and boulders, etc. The dykes in Nandurbar district are aligned in an ENE-WSW, N-S and WNW-ESE directions (CGWB, 2013). Water bearing formations in the study area are basalt (weathered/fractured/jointed vesicular/massive), and alluvium (sand and gravel) under semi-confined to confined conditions (CGWB, 2013; Deshpande, 1998).

Primarily there are two types of Deccan volcanic flows, “pahoehoe” and “aa” types (Deshpande, 1998), in the study area. In unconfined conditions, groundwater develops at shallow depths up to about 20 m mainly in the vesicular, fractured and jointed basalts. However in semi-confined to confined environment, groundwater aquifers are developed at deeper levels of about 40 m and beyond beneath the bole beds and massive basalts (CGWB, 2013). On the elevated plateau tops having good areal extent, local water table develops in top most layers and the wells in such areas show rapid decline water levels in post-monsoon season and go dry during peak summer. In the foot hills zone the water table is relatively shallow near the water courses and deep away from it and near the water divides. In the valleys and plains of river basin the water table aquifer occurs at shallow depth and the wells in such areas do not go dry and sustain perennial yield except in extreme summer or drought conditions (CGWB, 2013). It is reported that the yield of shallow depth dug wells fluctuates from 60 to 125 m^3/day while the variation in bore wells ranges from 2 to less than 20 m^3/day (CGWB, 2013). The yield of groundwater in the confined aquifers varies from 150 to 200 m3/day in the case of dug wells and 20 to 250 m3/day for bore wells (CGWB, 2013). In the present case shallow dug wells are yielding very higher than bore wells. This may be due to the fact that different flows of basalts were formed at different phases of eruption and the occurrence of fractures reduces with respect to flow i.e., the youngest flow has the maximum number of fractures, whereas, the oldest flow has the least or no fractures. Further, the incremental yields decline with depth (Asokan et al., 2014).

2.1. Dyke swarms of Nandurbar

The Nandurbar dyke swarms are ENE-WSW trending (Fig. 2a), tholeiitic type and are emplaced under regional crustal extension around 2.5 million years ago (Sheth et al., 2018). A rose diagram of the trends of 210 dykes of dolerite and basalt (>1 km) measured over this region shows their strong preferred direction (Fig. 2b). The dykes are intruded in the zeolitic compound pahoehoe flows which are highly weathered. These dykes may be vertically injected from shallow magma chambers, and others formed by lateral injection (Ray et al., 2007).

Much of the Nandurbar area is flat with elevation of more or less 200 m above mean sea level. The dykes being erosion-resistant than the basaltic rock, they form linear, often prominent ridges. In hand specimen, they appear aphyric and thin sections show common microphenocrysts of plagioclase, clinopyroxene or olivine.

The basalts are vesicular/amygdaloidal, jointed, fractured and compact. Alluvium and soil is exposed along the river and streams. The northern region consists of thick alluvium comprising of sand, silt, clay intercalations. The soil is coarse shallow, medium deep to deep black cotton. Towards north the soil is brownish to yellowish brown, coarse deep. The Tapi Valley consists of medium deep soils. The soil is derived from weathering of basalts. Water bearing layers are of weathered, fractured, jointed and vesicular basalt. Water occurs in alluvium with sands, silty clay lenses. Along the foothills the water table is shallow and becomes deeper with distance.

3. Materials and methods

3.1. VES data acquisition and analysis

Vertical electrical sounding (VES) data were measured from 39 sites (Fig. 2a) using Schlumberger electrode arrangement with IGIS made SSR-MP-AT instrument (Hyderabad). A maximum current electrode spread (AB) of 200 m was achieved on the basis of availability of sites due to the rugged topography. IPI2win inversion software (Bobachev, 2003) was used to process the field data. The sounding curves on log-log graph reveal 3–5 layered structure in the study area (Orellana and Mooney, 1966; Keller and Frischknecht, 1966). The root mean square (RMS) errors vary from 0.31–1.9%. One dimensional inversion results of a few representative VES curves are shown in Fig. 3. The primary geoelectric parameters (resistivity and thickness) obtained were then used to calculate the secondary geoelectric indicators (i.e. Dar Zarrouk parameters) like transverse resistance (T) and longitudinal conductance (S) (Maillet, 1947). These parameters helps in reducing the ambiguities associated with geoelectrical interpretation and therefore the hydrological properties of the aquifers can be deciphered with certain degree of confidence (Henriet, 1976). Other related geoelectric indices, i.e. transverse resistivity (ρ_t), longitudinal resistivity (ρ_l), electrical anisotropy (λ), fracture porosity (φ_f) and reflection coefficient (R_c) for all the 39 VES stations have been computed after (Zohdy et al., 1974) (Table 1).

If a prism of unit cross section which is characterized by its thickness “h” and resistivity “ρ” is considered, then the conductance (S) parallel to the face of prism and the resistance (T) normal to the face of the prism (Henriet, 1976) can be written as:

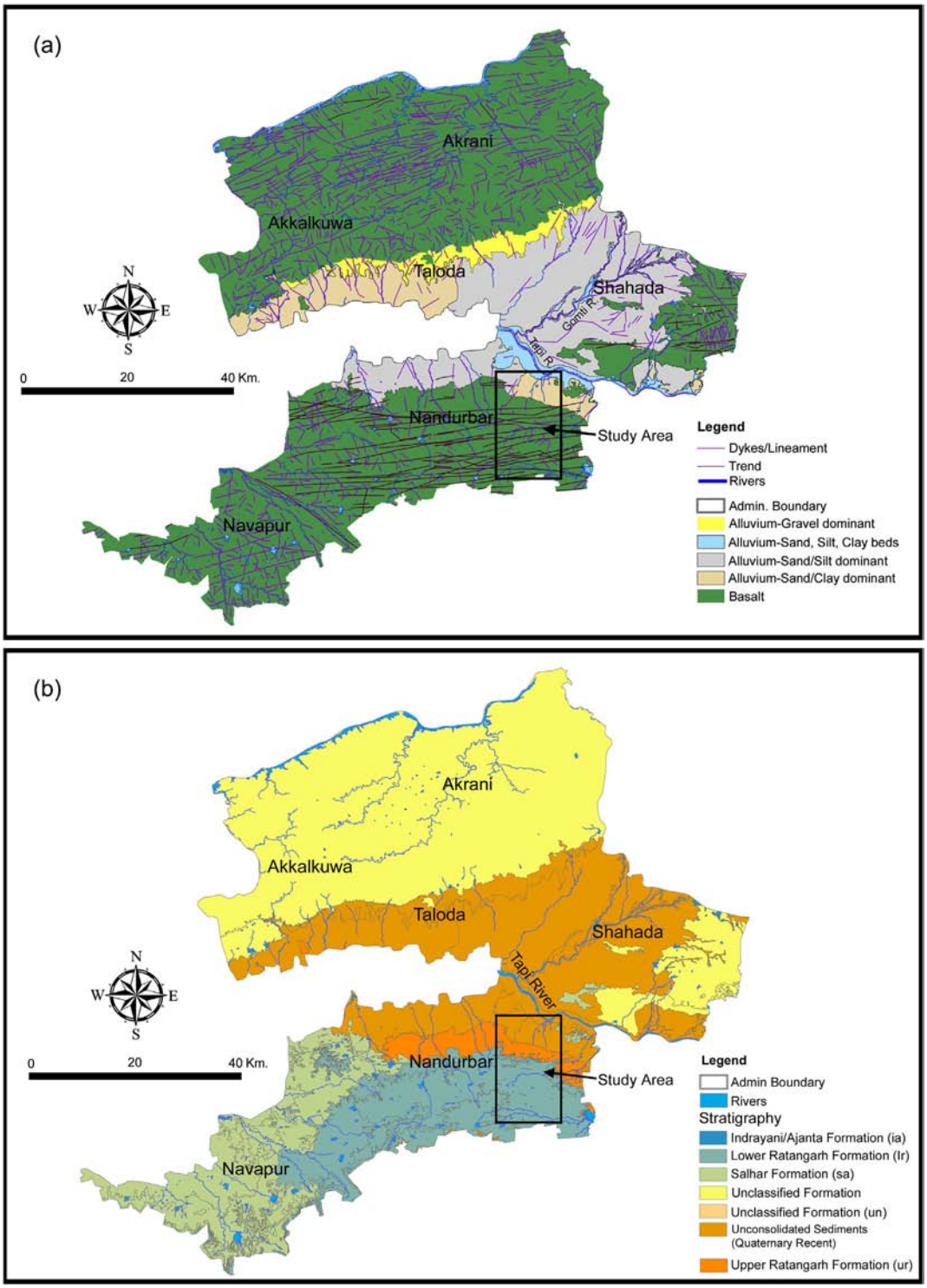

Fig. 1. (a) General geological map of Nandurbar district with study area marked on it. (b) Stratigraphy map of Nandurbar district with study area marked on it.

Total longitudinal conductance (S) is defined as,

$$S = \sum_{i=1}^{n} \frac{h_i}{\rho_i} \tag{1}$$

The total transverse resistance (T) is defined as,

$$T = \sum_{i=1}^{n} h_i \rho_i \tag{2}$$

Using Eq. (1), the longitudinal resistivity (ρ_l) of the current flowing parallel to the layers is given by,

$$\rho_l = \frac{H}{S} = \frac{\sum_{i=1}^{n} h_i}{\sum_{i=1}^{n} \frac{h_i}{\rho_i}} \tag{3}$$

where H represents the depth to the last geoelectric layer.

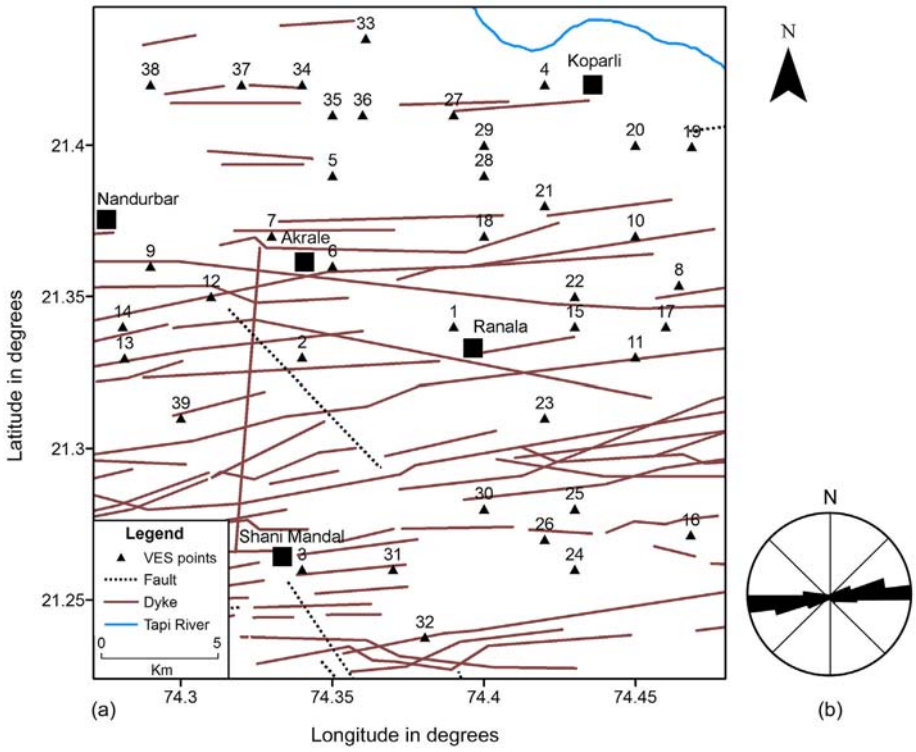

Fig. 2. (a) Location map of the study area showing the dykes, faults and VES surveying points. (b) Rose diagram showing preferred direction of the trends of 210 dykes in the study area.

Likewise, the transverse resistivity (ρ_t) of the current flowing perpendicular to the layers is deduced using Eq. (2) as,

$$\rho_t = \frac{T}{H} = \frac{\sum_{i=1}^{n} h_i \rho_i}{\sum_{i=1}^{n} h_i} \tag{4}$$

Combining Eqs. (3) and (4), the coefficient of anisotropy (λ) is given by,

$$\lambda = \sqrt{\rho_t / \rho_l} \tag{5}$$

Fracture porosities which are generally linked with tectonic fracturing of rocks were calculated using the expression derived by (Lane Jr. et al., 1995) as,

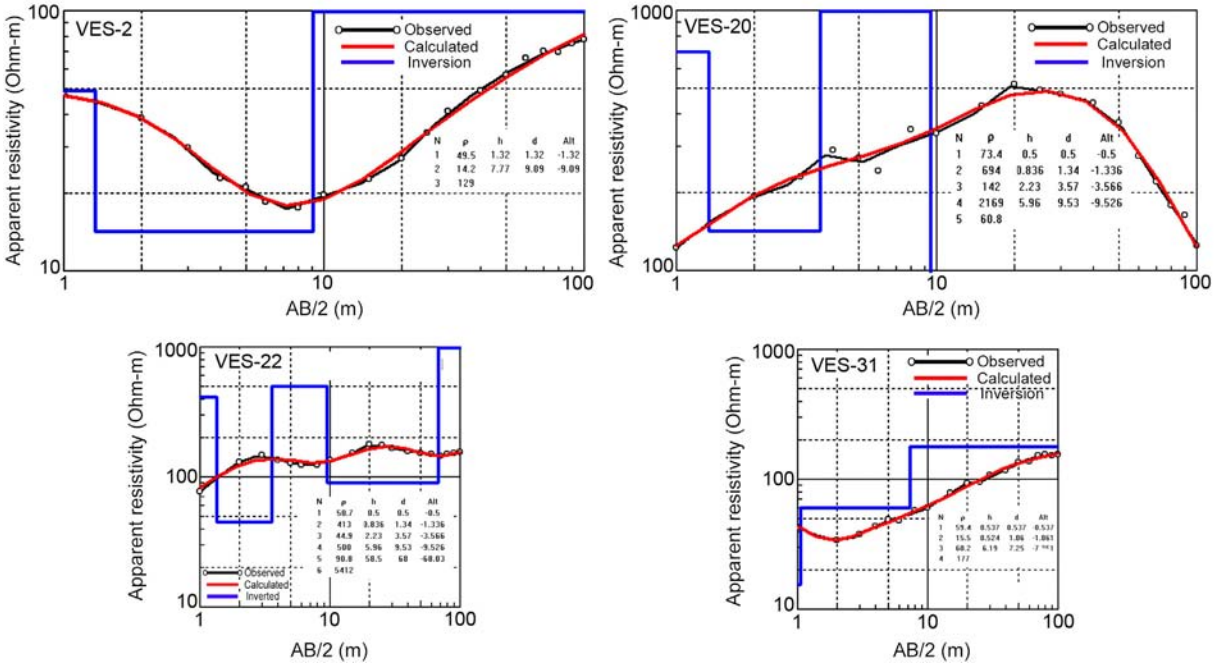

Fig. 3. One-dimensional inversion of representative VES curves.

Table 1
The computed geoelectric (Dar-Zarrouk) parameters for study area.

Sr. No.	Parameter	Min.	Max.	Average
1	Longitudinal conductance (S)	0.03	0.82	0.26
2	Trasverse resistance (Ωm^2)	126.60	87,907.80	6713.41
3	Transverse resistivity (Ωm)	19.43	4554.81	386.01
4	Longitudinal resistivity (Ωm)	12.76	364.62	87.20
5	Electrical anisotropy	1.00	4.03	1.75
6	Fracture porosity (%)	0.00001	0.484	0.044
7	Reflection coeff.	−0.998	0.993	−0.008

$$\varphi_f = \frac{3.41 \times 10^4 (N-1)\left(N^2-1\right)}{N^2 C(\rho_{max}-\rho_{min})} \quad (6)$$

here φ_f defines the fracture porosity; vertical anisotropy (N) relates to the coefficient of anisotropy (λ), as the vertical anisotropy is equal to the coefficient of anisotropy since for Schlumberger 1-D data, both (λ) and N are equal; ρ_{max} is the maximum and ρ_{min} is the minimum apparent resistivity in Ω-m and C is the specific conductance of groundwater in μS/cm. The specific conductance of groundwater from bore wells and dug wells in the study area were averaged to 610.5 μS/cm (CGWB, 2013).

It has been reported that reflection coefficient (k) divulges the extent of fracturing of the underlying basement (Olayinka, 1996; Olasehinde and Bayewu, 2011). It is reported that a low reflection coefficient reveals a weathered or fractured basement, indicating a higher water potential capacity (Olayinka, 1996). The reflection coefficient (k) was calculated as,

$$k = \frac{\rho_n - \rho_{(n-1)}}{\rho_n + \rho_{(n-1)}} \quad (7)$$

where ρ_n denotes the layer resistivity of the n^{th} layer and $\rho_{(n-1)}$ denotes the layer resistivity of overlying n^{th} layer.

Spatial variation maps of the above geoelectric indices were prepared using ArcGIS 10.5 software so as to understand the subsurface hydrogeological features. In order to prepare the base map of the study area, the geographic coordinates of respective VES stations were determined in the field using GARMIN N72 handheld GPS. These reference coordinates (longitudes and latitudes) were superimposed on satellite image (Google earth pro) of the study area in ArcGIS 10.5 to generate location base map (Fig. 2).

3.2. Spatial interpolation using Inverse Distance Weighted (IDW)

There are different data driven interpolation methods available like linear interpolation, Inverse Distance Weighted (IDW) interpolation, ordinary kriging and simple kriging interpolation, universal kriging interpolation, global polynomial interpolation, planar spline interpolation and local polynomial interpolation to name a few (Xiao et al., 2016). These schemes can generate representative spatial variation maps (Oliver and Webster, 1990). In the present study, however, Inverse Distance Weighted (IDW) interpolation technique via Spatial analyst tool in ArcGIS 10.5 is used to determine the spatial variation of the geoelectric parameters viz. longitudinal conductance, transverse resistance, longitudinal and transverse resistivities, electrical anisotropy, fracture porosity and reflection coefficient.

It has been reported that Inverse Distance Weighted (IDW) is an accurate spatial interpolation tool to estimate an unknown value at a location using some known values with corresponding weighted values (Xie et al., 2011). Further, IDW scheme requires adequate and well-spread data sampling points (Rabah et al., 2011). IDW algorithm is used to interpolate data spatially or to predict a value for any unsampled location in between the measured locations. Based on Tobler's assumption (Tobler, 1970), each estimated value in IDW interpolation scheme is a weighted average of the nearby sampling points. Weights are calculated by obtaining the inverse of the distance from an observation site to the location of the point being estimated (Burrough and McDonnell, 1998). Compared to other deterministic interpolation procedures, Burrough and McDonnell (1998) were of the view that using IDW with a squared distance term yielded results most consistent with original input data. This method is suitable for data sets where the maximum and minimum values in the interpolated surface commonly occur at sample points.

The kriging interpolation method, based on the linear and unbiased concept of mapping using semi-variogram model fitting technique, is the most popular interpolation schemes. This forms weights from surrounding measured values to predict unmeasured locations. Ordinary kriging not only presume the mean to be constant over the entire area, but also it is assumed to be constant in the local neighbourhood of each estimation point (Bohling, 2005). The benefit of using IDW interpolation technique over ordinary kriging scheme is that it calculates cell values by averaging the values of sample data points in the neighbourhood of each processing cell and the measured values closest to the unmeasured locations have the most influence. This technique calculates a value at a point of a region of a known semi-variogram without any previous information of the distribution mean. However IDW does not make explicit assumptions about the statistical properties of the input data, and the output value is limited to the range of the values used to interpolate. This means that the average can neither be more than the highest input value nor smaller than the lowest input value. Consequently, it cannot create ridges or valleys if these extremes have no longer already been sampled.

As mentioned earlier, in the present study, IDW interpolation technique is applied for spatial modelling of the various computed geoelectrical parameters. The parameter values were displayed using the classified renderer (geometrical interval scheme) in ArcGIS, while geometrical interval scheme was used to create class breaks. This allows generating stability between prominent changes in the middle values and the extreme values, so as to produce a result that is aesthetically captivating and cartographically extensive. The geoelectric parameters (longitudinal conductance, transverse resistance, longitudinal and transverse resistivities, electrical anisotropy, fracture porosity and reflection coefficient) for all the VES points are plotted in ArcGIS.

4. Results and discussion

4.1. Longitudinal conductance

The longitudinal conductance (S) provides facts concerning the disparity of the extremely resistive fresh basement topography as depth to the basement relates to S (Ayolabi et al., 2010). It has moreover been detailed that in an area where geoelectric environment are uniform, resistivity will not change much and hence S will be directly proportional to depth (H), suggesting that high S values are symptomatic of deeper basement and vice-versa (Gupta et al., 2015).

The spatial variation map of longitudinal conductance (S) for 39 VES stations in the study area is shown (Fig. 4a). The S value varies from 0.03 S (at VES 32) to 0.82 S (at VES 4). The northern and central part of the study area is encompassed with high *S* values (>0.49 S) at VES stations 2, 4, 22 and 23. Also, the northern part is covered by thick sequence of alluvium derived from River Tapi, suggestive of a deeper basement. The high *S* values observed in the central part of the study area follow the trend of *E*-W oriented dykes. The doleritic dykes in this area have deeper depth of weathering (Gupta et al., 2012) and therefore the high S values observed here could be attributed to enhanced groundwater potential zones.

It is reported that clayey overburden is characterized by high longitudinal conductance, which protects the underlying aquifer from contaminants (Oladapo et al., 2004; Oladapo and Akintorinwa, 2007). The earth acts as a natural filter to these contaminants from seeping through

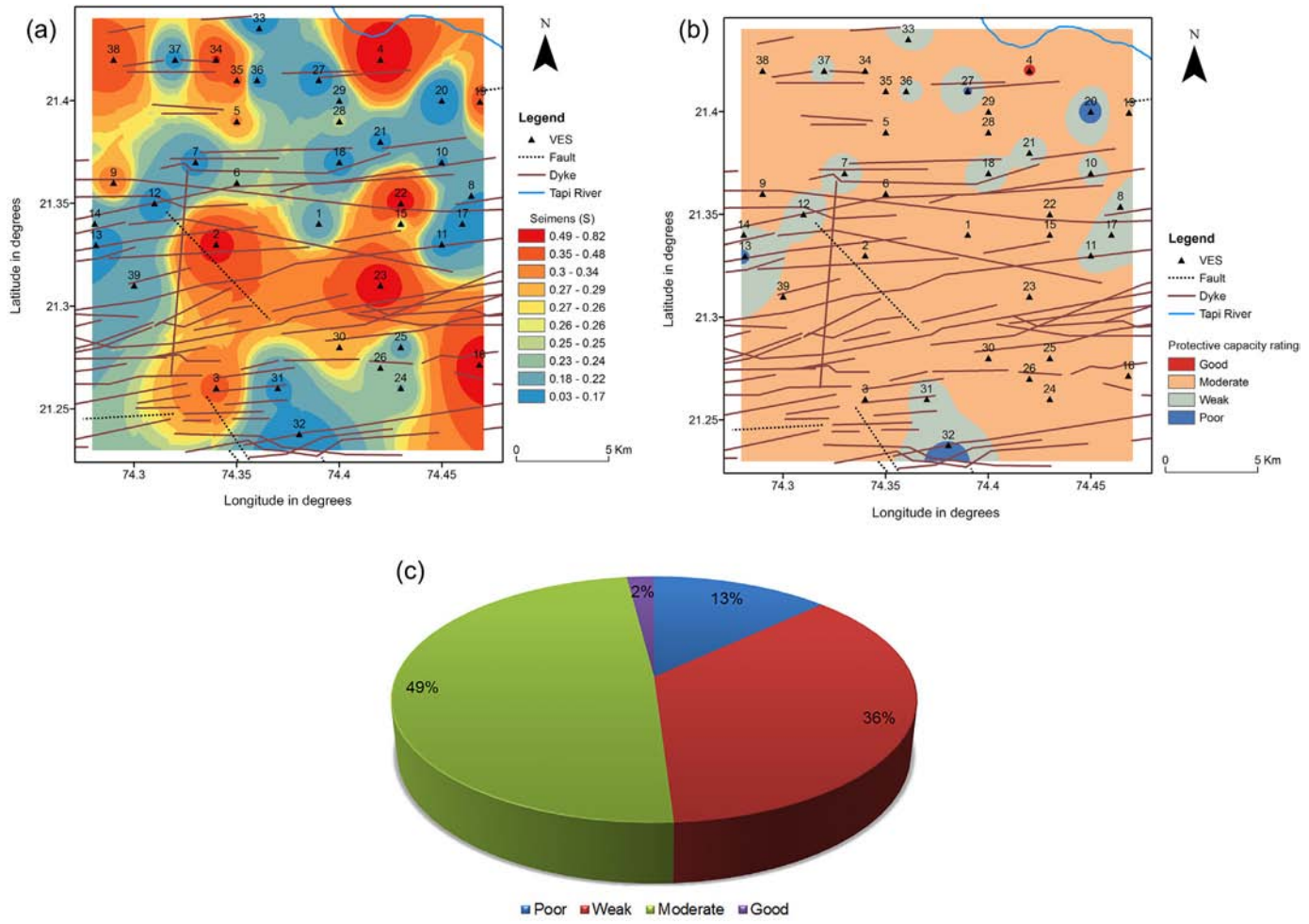

Fig. 4. (a) Spatial distribution of longitudinal conductance (S) in the study area. (b) Spatial distribution of Aquifer protective capacity in the study area. (c) Pie diagram showing the protective capacity of aquifers in the study area.

and its ability to check the infiltrating contaminants is a measure of its protective capacity. A modified classification of aquifer protective capacity rating is given by Oladapo et al. (2004), which facilitate to categorize an area into poor, weak, moderate, good, very good and excellent protective capacity zones (Table 2).

The aquifer protective capacity of the study area is assessed based on the longitudinal conductance (S) values and is shown in Fig. 4b. The S values (<0.1 S) evident at VES stations 13, 17, 20, 27, and 32 signifies poor aquifer protective capacity rating. The northern and at a few central sites covering stations 1, 7–8, 10–12, 14, 18, 21, 31, 33, 36–37 and 39 reveal S values in the range 0.1 to 0.19 S, indicating weak aquifer protective capacity rating. S values (0.2 to 0.79) are observed at VES point 2–3, 5–6, 9, 15–16, 19, 22–26, 28–29, 30, 34–35 and 38 suggesting moderate aquifer protective capacity rating due to the weathering effect of the dyke swarms. However good aquifer protective capacity is observed only at VES 4 (0.82 S), which is located around 1.5 km south of the River Tapi and is thus expected to have a thick sequence of alluvial deposit, thereby offering protection to the underlying aquifers.

Therefore, the protective capacity of aquifers in the study area reveals that about 2% area falls under the "good" aquifer protective capacity, while 49% is observed to have "moderate" aquifer protective capacity. A total of 36% is characterized by "weak" and 13% as "poor" aquifer protective capacity ratings (Fig. 4c).

Table 2
Modified longitudinal conductance/protective capacity ratings. After Oladapo et al. (2004).

Longitudinal conductance (seimens)	Protective capacity rating
>10	Excellent
5–10	Very good
0.8–4.9	Good
0.2–0.79	Moderate
0.1–0.19	Weak
<0.1	Poor

4.2. Transverse resistance

The transverse resistance (T) values in the study area vary from 126.6 Ωm^2 (at VES 15) to 87,907.8 Ωm^2 (at VES 13) (Fig. 5). It can be noted from Fig. 5 that low T values (<4700 Ωm^2) are associated with low resistivity material such as clay/silt/weathered formations. High T values (up to 28,000 Ωm^2) trending NE-SW and N-S, which also follow the direction of the major dyke swarms, are encompassing VES stations 6, 13, 18, 20, 21, 24, 28 and 34 in the study area, signaling fresh water zone. Very high T values at VES 13 and 18 (>28,000 Ωm^2) signify very high resistive formations (massive basalts and dyke intrusions) in the subsurface. It is envisaged that increasing T values indicate high transmissivity of aquifers and are associated with zones of high transmissivity and, therefore highly permeable to fluid movement (Braga et al., 2006).

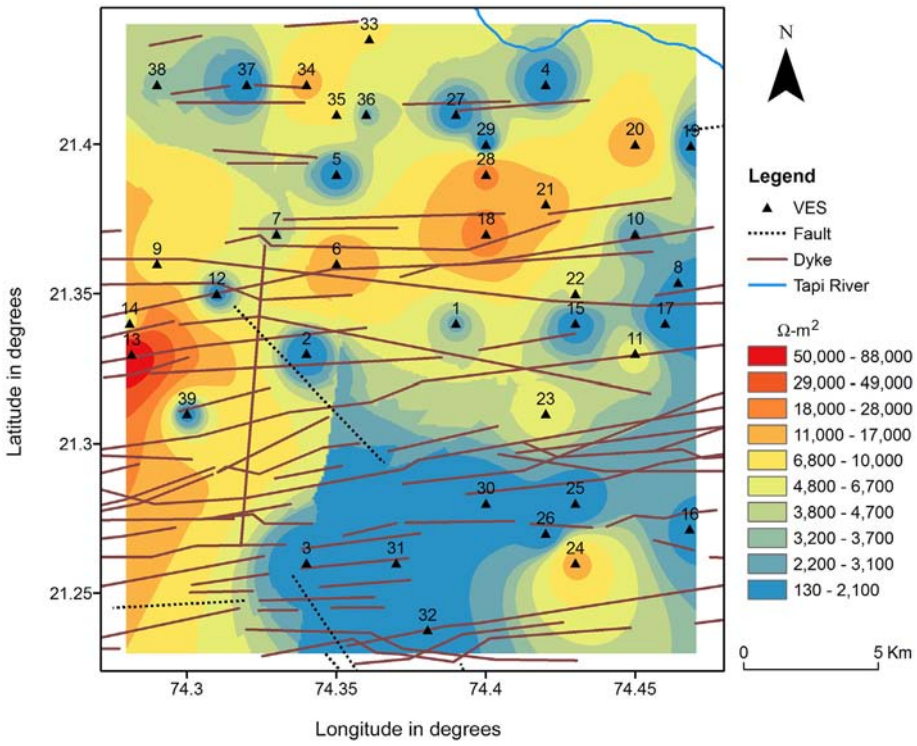

Fig. 5. Spatial distribution of transverse resistance (T) in the study area.

4.3. Transverse resistivity and longitudinal resistivity

The spatial distribution of transverse resistivity (ρ_t) is shown in Fig. 6a. The $\rho_t$value varies from a minimum of 19.43 Ωm at VES 2 to a maximum of 4554.81 Ωm at VES 13. From the figure it can be inferred that low ρ_t values are observed at almost all the VES stations towards north. The low ρ_t at VES 4 is due to the sediments of Tapi River basin, while low resistivity observed at VES stations 29, 27, 5, 36, 35, 34, 37 and 38 could be due to the weathered dyke swarms present. High ρ_t values (>1000 Ωm) are observed towards west and north eastern part of study area covering VES stations 13 (4554.81 Ωm), 20 (1825.12 Ωm) and 28 (1158.18 Ωm).

The spatial distribution of longitudinal resistivity (ρ_l) is shown in Fig. 6b. The $\rho_l$value ranges from a minimum of 12.76 Ωm at VES 15 to a maximum of 364.62 Ωm at VES 18. It is revealed that high ρ_l values (>240 Ωm) are observed at west and north eastern part of study area covering VES stations 13 (285.23 Ωm), 18 (364.62 Ωm) and 20 (283.62 Ωm).

The transverse resistivity is usually more than the longitudinal resistivity in heterogeneous medium (Flathe, 1955). This implies that the current flow and average hydraulic conduction along the longitudinal boundary is greater than those normal to the boundary plane (Ayolabi et al., 2010). Keller (1982) opined that longitudinal resistivity is subjugated by the more conductive layers (in the present case, clay and

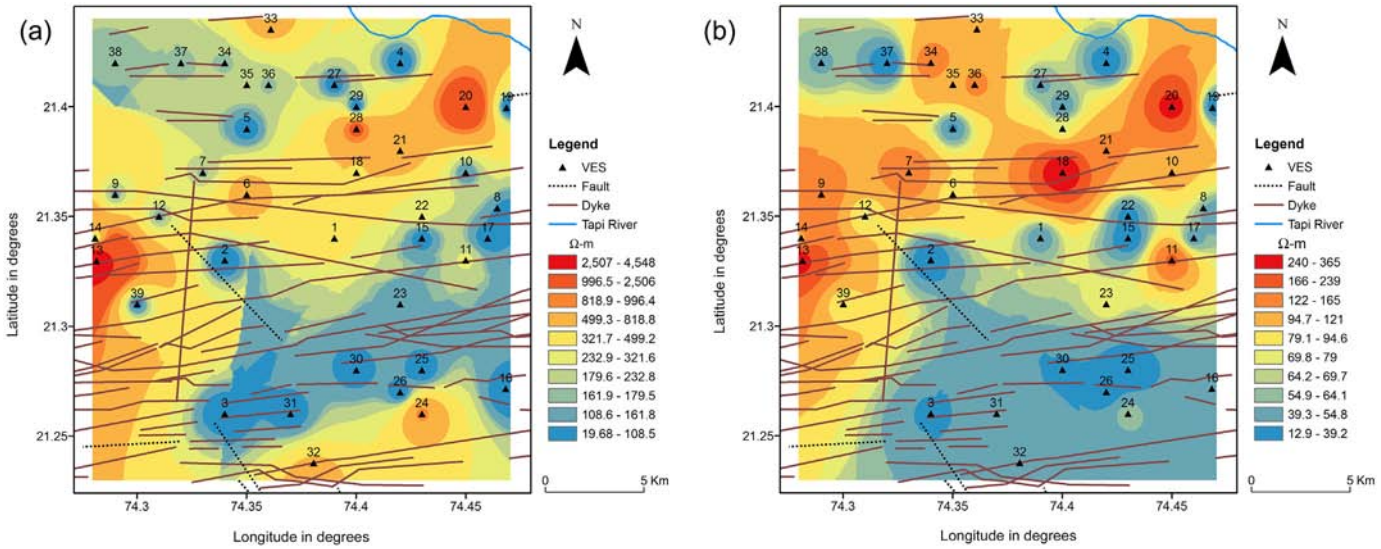

Fig. 6. (a) Spatial distribution of transverse resistivity (ρ_t) in the study area. (b) Spatial distribution of longitudinal resistivity (ρ_l) in the study area.

weathered/fractured basalts), whereas transverse resistivity increases rapidly even if a small fraction of resistive layers are present.

4.4. Electrical anisotropy

The value of electrical anisotropy (λ) ranges from 1 to 4.02 with an average value of 1.75. The coefficient of anisotropy is generally 1 and rarely exceeds 2 in most of the geologic environments. The λ value increases as the hardness and compactness of rock increases. This is indicative of low porosity and permeability medium. The λ value between 1 and 1.5 signify potential zone for fresh water aquifer.

As can be seen from Fig. 7, total of 26 VES sites in the study area reveals λ value around 1–1.5. In the study area, VES stations (2, 3, 5, 7, 9, 12, 31 and 39) around N-S dyke and other VES stations (8, 10, 16, 26, 27 and 36) suggest potential aquifer zones (Fig. 7). It can therefore be construed that the areas having least water table fluctuation is related with low λ values and higher water table fluctuation regions are linked with high λ values.

The coefficient of anisotropy (Fig. 7) reveals an increasing tendency from NE to SW direction with high λ value (>2) at the VES stations 20, 28, 6 and 13. A conspicuous NW-SE oriented high λ value (>1.9) is also revealed at VES stations 33, 6, 1 and 24. These highs are the signatures of the EW and NS oriented dyke features as marked on Fig. 7, indicating the heterogeneous and anisotropic nature of the subsurface in both NE-SW and NW-SE directions.

4.5. Fracture porosity

The fracture porosity (φf) values divulge higher porosities at the northwestern, central and southeastern part of the study area (Fig. 8). A maximum porosity value of 0.48 was observed in the northwestern part at VES 37. Minimum porosity value of 0.000001 (VES 39) is seen at the southwestern part. A positive correlation between the fracture porosity values with the high and low values of electrical anisotropy (λ) is observed in the present study (Fig. 9).

4.6. Reflection coefficient

The reflection coefficient (k) can give an understanding about the aquiferous nature of the basement rocks thereby indicating areas of high density water filled fractures. The spatial variation of reflection coefficient (k) is contoured and shown in Fig. 10. The k value in the study area varies from a minimum of −0.99 at VES 6, 21, 24, 28 and 35 to a maximum of 0.98 at VES 22.

The central and northern parts of study area show negative k values. NE-SW trend of low reflection coefficient is observed covering VES 20, 21, 28, 18, 1 and 6. Another NE-SW low trend is evident in northwestern side of the study area. These low reflection coefficient trends are coinciding with the major dykes of the region. Tahama et al. (2019) is of view that the negative value of reflection coefficient indicates the dominancy of weathered and fractured zones having a low resistivity below a high resistivity groundwater repository, however in the present study; negative k values are associated with carrier type of dykes.

It is observed that areas with low reflection coefficient (k) values correspond to high λ values (Fig. 11). Thus, it may be construed that lower reflection coefficient values is observed where the electrical anisotropy is high, suggesting an inverse relationship between these two indices. This also reflects that the subsurface is composed of weathered/fractured rocks, which has better water holding capacity.

5. Conclusions

The Nandurbar area in northern Maharashtra is characterized by copious gabbroic and doleritic dykes intruded into the basaltic lava flows. These are parallel to sub parallel bodies forming linear ridges of moderate relief. They are partly exposed and partly concealed, thus affecting the local topography. In general ENE-WSW and E-W trending dykes are dominant followed by NW-SE ones. Vertical electrical soundings carried out at 39 sites to decipher the anisotropic character of the dykes and the protective capacity of the aquifers. The longitudinal conductance (S) and transverse resistance (T) along with other

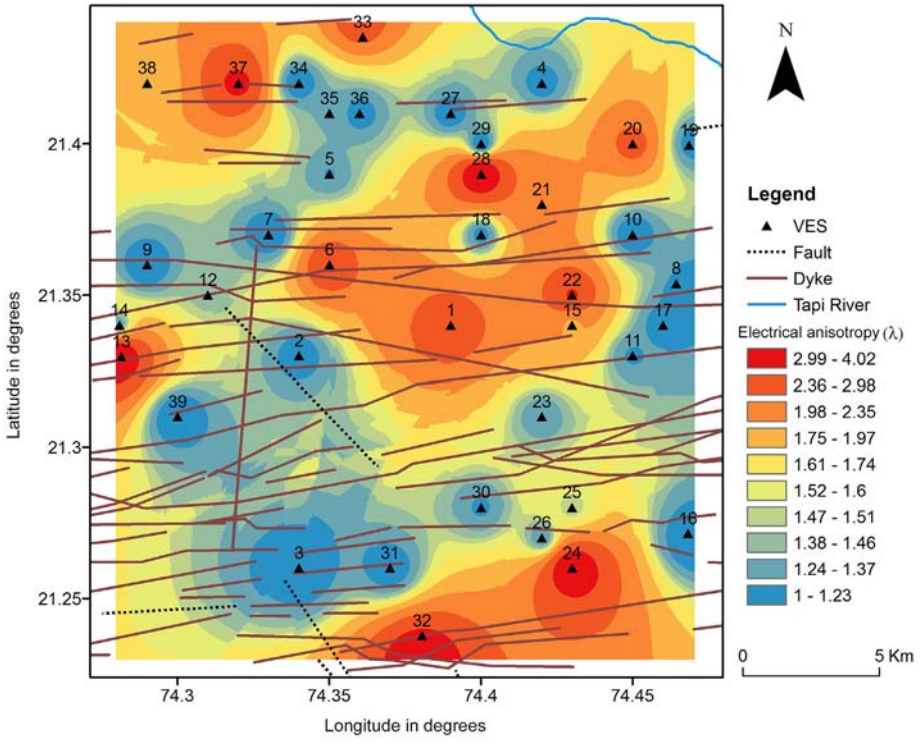

Fig. 7. Spatial distribution of electrical anisotropy (λ) in the study area. The lineaments are also marked on the map.

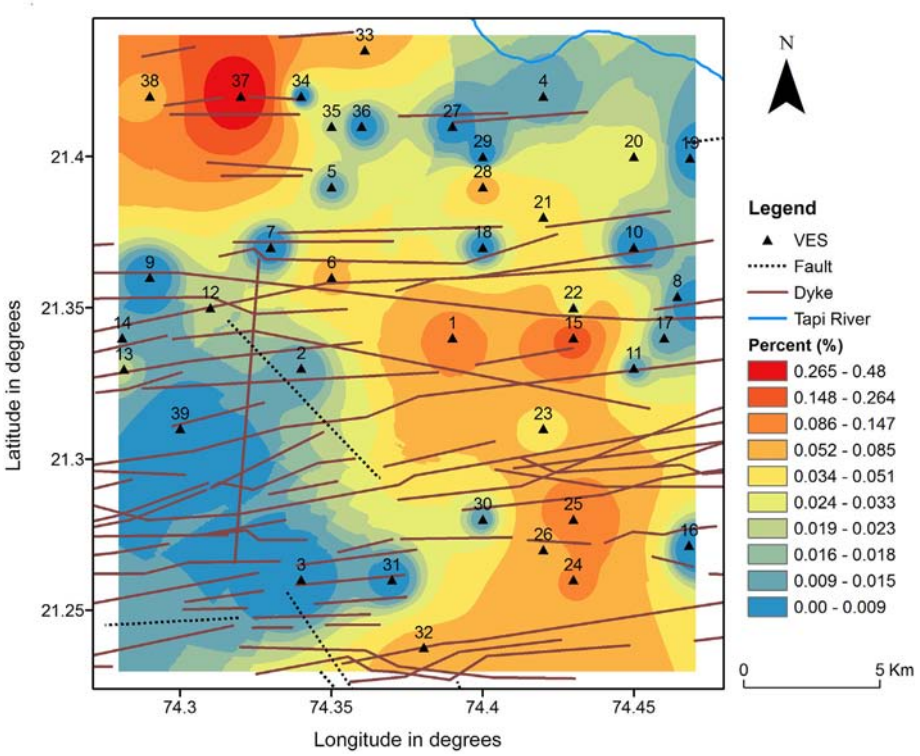

Fig. 8. Spatial distribution of fracture porosity (φf) in the study area.

geoelectrical indices were computed utilizing the resistivity and layer thickness at each station. The Inverse Distance Weighted (IDW) algorithm was used to obtain the spatial variation of all the geoelectric parameters. From the longitudinal conductance values, 49% of the area reveals poor to weak aquifer protective capacity rating, while 49% and 2% shows moderate and good aquifer protective capacity rating respectively. This implies that the study area has a comparatively poor to moderate aquifer protective capacity rating. The weaker zones are thus prone to infiltrating contaminants. The electrical anisotropy λ varies from 1 to 4.02 with an increasing trend from NE to SW direction. Also, NW-SE oriented high λ value (>1.9) is evident at a few VES stations (33, 6, 1, and 24). The high λ values are the impressions of the EW and NS oriented dykes, suggestive of the heterogeneous and anisotropic behavior of the subsurface in the study area. The intersection points of several dykes towards north and south with λ value 1–1.5, implies potential zone for groundwater recharge. A positive relationship is revealed between the fracture porosity and electrical anisotropy, while a negative correlation is seen between reflection coefficient and electrical anisotropy. The IDW algorithm presented a precise and consistent approximation of the spatial variation and the underlying heterogeneities.

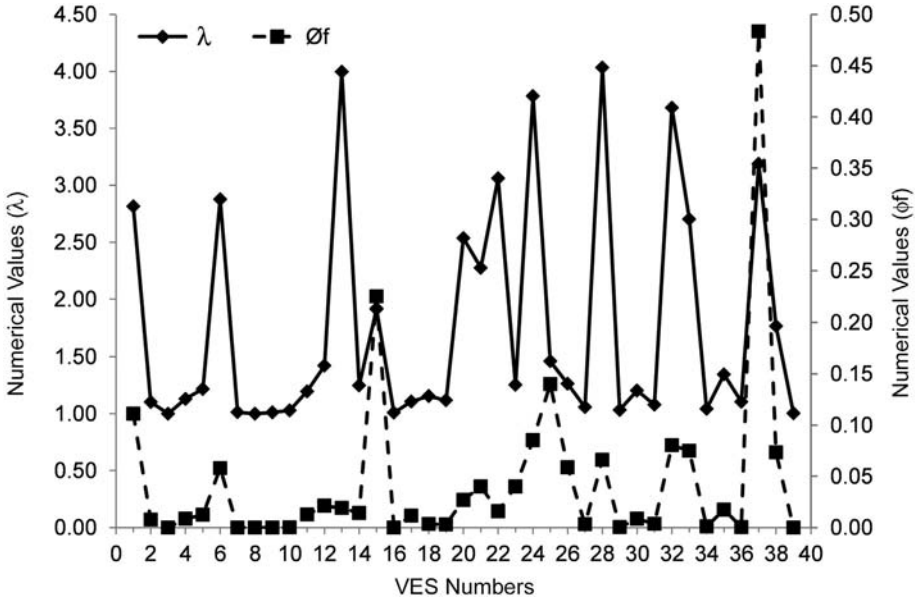

Fig. 9. Plot of coefficient of anisotropy (λ) and fracture porosity (φf) with VES numbers.

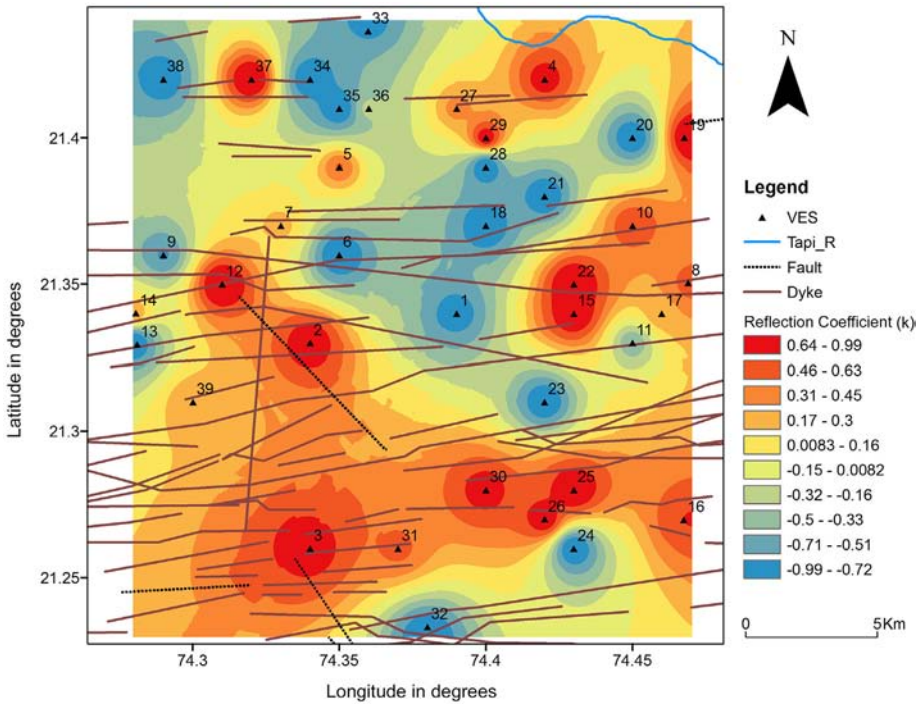

Fig. 10. Spatial distribution of reflection coefficient (k) in the study area.

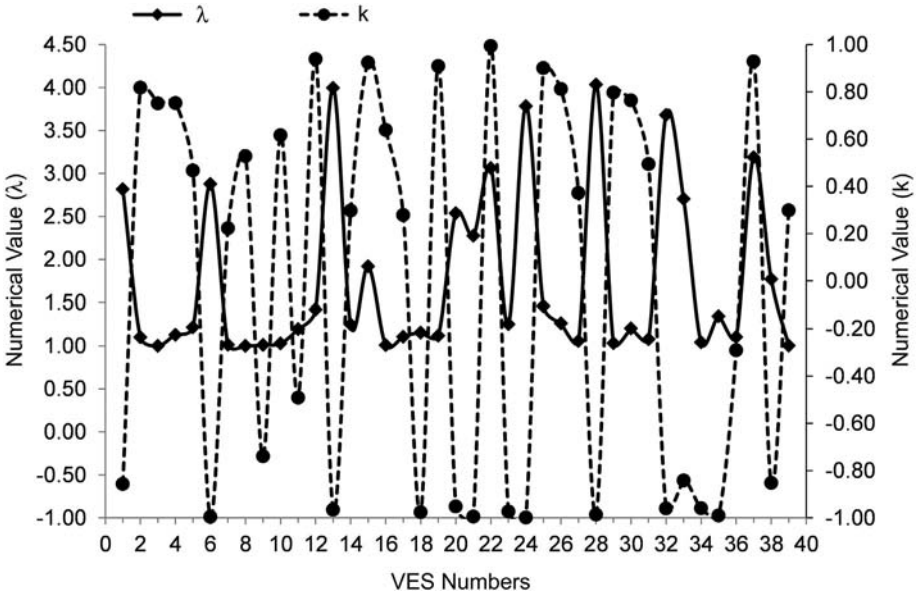

Fig. 11. Plot of coefficient of anisotropy (λ) and reflection coefficient (k) with VES numbers.

The estimation of protective capacity rating of the aquifers is critical from the viewpoint of contamination. It can be concluded that if dykes possess sufficient width, length and favourable hydrogeological structure, they can form potential and distinct aquifers.

Submission declaration

The work described here has not been published previously, that it is not under consideration for publication elsewhere, that its publication is approved by all authors and tacitly or explicitly by the responsible authorities where the work was carried out, and that, if accepted, it will not be published elsewhere including electronically in the same form, in English or in any other language, without the written consent of the copyright-holder.

Authors' contributions

The first author, Ms. Khan Tahama, has carried out the analysis of VES data and computed the various geoelectrical indices and prepared the spatial distribution maps using Inverse Weighted Distance technique for the first time. She has interpreted the dataset and written the manuscript.

The second author, Ms. Arti Baride, was involved in field surveys and has contributed in providing inputs with respect to geology and hydrogeology of the study region, used in the manuscript.

The third author (Dr. Gautam Gupta, (CA)) was instrumental in conceiving and guiding the research program, data acquisition, interpretation and editing the manuscript.

The fourth author, Dr. Vinit C. Erram has participated and executed the field surveys.

The fifth author (Dr. Mukund V. Baride) participated in the field works and has helped in a substantial way by providing his expertise in hydrogeological processes in hard-rock terrain.

Role of the funding source

The study was funded in house by Indian Institute of Geomagnetism.

Availability of data and material

The vertical electrical sounding data was acquired from field survey by the authors.

Code availability

The resistivity data was processed and analyzed using IPI2WIN (Version 3.0.1, a 7.01.03) developed by Bobachev, A., Moscow State University and is duly acknowledged.

Declaration of Competing Interest

The authors hereby declare that we have no conflict of interest.

Acknowledgements

The authors express their gratitude to Dr. D.S. Ramesh, Director, Indian Institute of Geomagnetism, Panvel for granting permission to publish the work. Authors are thankful to Dr. M. Laxminarayana for assisting in field work. The authors express their appreciation to Shri Shubhankar Das, Department of Geography, Mumbai University, for help in map preparations in ArcGIS environment.

References

Asokan, A., Benjamin Vedanayagam, J., Sivaramakrishnan, J., 2014. Ground water occurrence and management in basalts of Afzalpur taluk, Gulbarga district, Karnataka. Proc. of National workshop on "Water conservation retrospect & prospects", CGWB, Bangalore, India, pp. 114–151.

Auden, J.B., 1949. Dykes in western India. Trans. Nat'l. Inst. Sci. India 3, 123–157.

Ayolabi, E.A., Folorunso, A.F., Oloruntola, M.O., 2010. Constraining causes of structural failure using Electrical Resistivty Tomography (ERT): a case study of Lagos, Southwestern, Nigeria. Miner. Wealth 156, 7–18.

Babiker, M., Gudmundsson, A., 2004. The effects of dykes and faults on groundwater flow in an arid land: the Red Sea Hills, Sudan. J. Hydrol. 297, 256–273.

Batayneh, A.T., 2013. The estimation and significance of Dar-Zarrouk parameters in the exploration of quality affecting the Gulf of Aqaba coastal aquifer systems. J. Coast. Conserv. 17, 623–635.

Bobachev, A., 2003. Resistivity Sounding Interpretation, IPI2WIN. Version 3.0.1, A 7.01.03. Moscow State University.

Bohling, G., 2005. Introduction to geostatistics and variogram analysis. Kansas Geol. Surv. Lawrence KS USA, pp. 1–20.

Braga, A.C.O., Filho, W.M., Dourado, J.C., 2006. Resistivity (DC) method applied to aquifer protection studies. Brazil. J. Geophys. 24 (4), 573–581.

Burrough, P.A., McDonnell, R.A., 1998. Principles of Geographical Information Systems. second ed. Clarendon Press, Oxford.

Central Ground Water Board (CGWB), 2013. Manual on Hydrogeology of Nandurbar District, Maharashtra, Technical Report No. 1797/DBR/2013.

Deshpande, G.G., 1998. Geology of Maharashtra. Geological Society of India, Bangalore.

Duraiswami, R.A., 2005. Dykes as potential groundwater reservoirs in semi-arid areas of Sakri Taluka, District Dhule of Maharashtra. Gondwana Geol. Mag. 20 (1), 1–9.

Erram, V.C., Gupta, G., Pawar, J.B., Kumar, S., Pawar, N.J., 2010. Potential groundwater zones in parts of Dhule District, Maharashtra: a joint interpretation based on resistivity and magnetic data. J. Ind. Geol. Congr. 2 (1), 37–45.

Flathe, H., 1955. Possibilities and limitations in applying geoelectrical methods to hydrogeological problems in the coastal area of Northwest Germany. Geophys. Prospect. 3, 95–110.

Geological Survey of India (GSI), 2001. District Resource Map – Dhule-Nandurbar District, Maharashtra. Geol. Surv, India.

Gupta, G., Erram, V.C., Kumar, S., 2012. Temporal geoelectric behavior of dyke aquifers in Northern Deccan Volcanic Province India. J. Earth Syst. Sci. 121 (3), 723–732.

Gupta, G., Patil, S.N., Padmane, S.T., Erram, V.C., Mahajan, S.H., 2015. Geoelectric investigation to delineate groundwater potential and recharge zones in Suki river basin, North Maharashtra. J. Earth Syst. Sci. 124 (7), 1487–1501.

Henriet, J.P., 1976. Direct application of the Dar-Zarrouk parameters in ground water surveys. Geophys. Prospect. 24, 344–353.

Keller, G.V., 1982. Electrical properties of rocks and minerals. In: Carmichael, R.S. (Ed.), Hand Book of Physical Properties of Rocks. CRC Press, pp. 217–293.

Keller, G.V., Frischknecht, F.C., 1966. Electrical Methods in Geophysical Prospecting. Pergamon Press Inc, Oxford.

Kumar, D., Rai, S.N., Thiagarajan, S., Ratnakumari, Y., 2011. Evaluation of heterogeneous aquifers in hard rocks from resistivity sounding data in parts of Kalmeshwar taluk of Nagpur district, India. Curr. Sci. 107 (7), 1137–1145.

Lane Jr., J.W., Haeni, F.P., Watson, W.M., 1995. Use of a square array direct current resistivity method to detect fractures in crystalline bedrock in New Hampshire. Ground Water 33 (3), 476–485.

Loke, M.H., 2000. Electrical Imaging Surveys for Environmental and Engineering Studies, A Practical Guide to 2-D and 3-D Surveys. https://www.academia.edu/11991713/.

Maillet, R., 1947. The fundamental equation of electrical prospecting. Geophysics 12, 529–556.

Maiti, S., Gupta, G., Erram, V.C., Tiwari, R.K., 2013. Delineation of shallow resistivity structure around Malvan, Konkan region, Maharashtra by neural network inversion of vertical electrical sounding measurements. Environ. Earth Sci. 68, 779–794.

Melluso, L., Sethna, S.F., Morra, V., Khateeb, A., Javeri, P., 1999. Petrology of the mafic dyke swarm of the Tapti River in the Nandurbar area (Deccan Volcanic Province). Mem. Geol. Soc. India 43, 735–755.

Mondal, N.C., Singh, V.P., Ahmed, S., 2013. Delineating shallow saline groundwater zones from Southern India using geophysical indicators. Environ. Monit. Assess. 185, 4869–4886.

Nilsen, K.H., Sydnes, M., Gudmundsson, A., Larsen, B.T., 2003. How dykes affect groundwater transport in the northern part of the Oslo Graben. Geophys. Res. Abstracts 5, 09684.

Oladapo, M.I., Akintorinwa, O.J., 2007. Hydrogeophysical study of Ogbese Southwestern, Nigeria. Global J. Pure Appl. Sci. 13 (1), 55–61.

Oladapo, M.I., Mohammed, M.Z., Adeoye, O.O., Adetola, B.A., 2004. Geoelectrical investigation of the Ondo State Housing Corporation Estate Ijapo Akure, southwestern Nigeria. J. Min. Geol. 40 (1), 41–48.

Olasehinde, P.I., Bayewu, O.O., 2011. Evaluation of electrical resistivity anisotropy in geological mapping: a case study of Odo Ara, West Central Nigeria. Afr. J. Environ. Sci. Tech. 5 (7), 553–566.

Olayinka, A.I., 1996. Non uniqueness in the interpretation of bedrock resistivity from sounding curves and its hydrological implications. Water Resour. J. NAH 7 (1–2), 55–60.

Oliver, M.A., Webster, R., 1990. Kriging: a method of interpolation for geographical information systems. Int. J. GIS 4 (3), 313–332.

Orellana, E., Mooney, H.M., 1966. Master Tables and Curves for Vertical Electrical Sounding over Layered Structures. Interciencia, Madrid, Spain.

Patil, S.K., Rao, D.R.K., 2002. Palaeomagnetic and rock magnetic studies on the dykes of Goa, west coast of Indian Precambrian Shield. Phys. Earth Planet. Inter. 133, 111–125.

Pawar, N.J., Pawar, J.B., Supekar, A., Karmalkar, N.R., Kumar, S., Erram, V.C., 2008. Deccan dykes as discrete and prospective aquifers in parts of Narmada Tapi zone, Dhule District, Maharashtra. In: Srivastava, R.K., Sivaji, Ch., Chalapati Rao, N.V. (Eds.), Indian Dykes, GSI Special Volume. Narosa Publishing House Pvt. Ltd, New Delhi India, pp. 189–198.

Rabah, F.K.J., Ghabayen, S.M., Salha, A.A., 2011. Effect of GIS interpolation techniques on the accuracy of the spatial representation of groundwater monitoring data in Gaza strip. J. Environ. Sci. Technol. 4 (6), 579–589.

Rai, S.N., Thiagarajan, S., Ratnakumari, Y., Anand Rao, V., Manglik, A., 2013. Delineation of aquifers in basaltic hard rock terrain using vertical electrical soundings data. J. Earth Syst. Sci. 122 (1), 29–41.

Ray, R., Sheth, H.C., Mallik, J., 2007. Structure and emplacement of the Nandurbar-Dhule mafic dyke swarm, Deccan Traps, and the tectono magmatic evolution of flood basalts. Bull. Volcano 69, 531–537.

Sethna, S.F., Khateeb, A., Javeri, P., 1996. Petrology of basic intrusives in Deccan Volcanic Province south of Tapti Valley and their comparison with those along West Coast. Gond. Geol. Mag. 2, 225–232.

Shailaja, G., Gupta, G., Suneetha, N., Laxminarayana, M., 2019. Assessment of aquifer zones and its protection via second-order geoelectric indices in parts of drought-prone region of Deccan Volcanic Province, Maharashtra, India. J. Earth Syst. Sci. 128, 78. https://doi.org/10.1007/s12040-019-1104-y.

Sheth, H.C., Vanderkluysen, L., Demonterova, E.I., Ivanov, A.V., Savatenkov, V.M., 2018. Geochemistry and 40Ar/39Ar geochronology of the Nandurbar-Dhule mafic dyke swarm: dyke-sill-flow correlations and stratigraphic development across the Deccan flood basalt province. Geol. J. 1-20. https://doi.org/10.1002/gj.3167.

Singh, R.P., Jamal, A., 2002. Dykes as groundwater loci in parts of Nashik District, Maharashtra. J. Geol. Soc. India 59 (2), 143–146.

Suneetha, N., Gupta, G., Tahama, K., Erram, V.C., 2020. Two-dimensional modelling of electrical resistivity imaging data for assessment of saline water ingress in coastal aquifers of Sindhudurg district, Maharashtra, India. Model. Earth Syst. Environ. https://doi.org/10.1007/s40808-020-00725-w.

Tahama, K., Gupta, G., Baride, M.V., Patil, J.B., Baride, A., 2019. Evaluation of groundwater potential and aquifer protective capacity of the overburden units in trap covered Dhule District, Maharashtra. Bull. Pure Appl. Sci. 38F (2), 246–265.

Tobler, W.R., 1970. A computer movie simulating urban growth in the detroit region. Econ. Geog. 46, 234–240 Supplement: Proceedings, International Geographical Union. Commission on Quantitative Methods.

Xiao, Y., Gu, X., Yin, S., Shao, J., Cui, Y., Zhang, Q., Niu, Y., 2016. Geostatistical interpolation model selection based on ArcGIS and spatio-temporal variability analysis of groundwater level in piedmont plains, northwest China. SpringerPlus 5, 425. https://doi.org/10.1186/s40064-016-2073-0.

Xie, Y.F., Chen, T.B., Lei, M., Yang, J., Guo, Q.J., Song, B., Zhou, X.Y., 2011. Spatial distribution of soil heavy metal pollution estimated by different interpolation methods: accuracy and uncertainty analysis. Chemosphere 82 (3), 468–476.

Zohdy, A.A.R., Eaton, G.P., Mabey, D.R., 1974. Application of Surface Geophysics to Ground-water Investigation, Second ed. Techniques of Water-resources Investigations Series of the United States Geological Survey.